Development of a non-adiabatic Flamelet model for reacting flows with heat loss

Nikolaos Perakis [(1)], Christof Roth [(1)], Oskar J. Haidn [(1)]

[(1)]Chair of Turbomachinery and Flight Propulsion, Technische Universität München
Boltzmannstraße 15, 85748 Garching, Germany
nikolaos.perakis@ltf.mw.tum.de

KEYWORDS: CFD, Flamelet, methane, wall heat flux, non-adiabatic

ABSTRACT

The current work presents the extension of the Flamelet model for turbulent combustion calculations to account for deviations from adiabatic conditions. The aforementioned extension is expected to significantly improve the prediction of the chemical processes occurring in the vicinity of cooled walls in rocket engine applications. A lower enthalpy level leads to an increase of the recombination reactions, which is of particular interest in the case of methane/oxygen combustion. Two different methods for including the non-adiabatic effects in the Flamelet model are presented and compared to each other. In the first method a source term is applied to the energy equation in the calculation of the counterflow diffusion flame. In the second approach, the Flamelet equations are solved in mixture fraction space and the energy equation is replaced by a prescription of the enthalpy profile. A new procedure using a splitting algorithm is proposed for the solution of the resulting boundary value problem. The two approaches were found to deliver almost identical results when the unity Lewis number method was used for the diffusion coefficients. Comparing the non-adiabatic results with the frozen Flamelet ones showed the importance of the recombination reactions at lower enthalpy levels. An increased temperature and wall heat flux are shown to result after consideration of the non-adiabatic effects.

NOMENCLATURE

c_p	: specific heat capacity [$\mathrm{J/(kg \cdot K)}$]
h	: specific enthalpy [$\mathrm{J/kg}$]
i	: iteration index [-]
j	: diffusive flux [$\mathrm{1/(m^2 \cdot s)}$]
J	: Jacobi matrix [$\mathrm{m^3/(s \cdot kg)}$]
M	: molecular weight [$\mathrm{kg/mol}$]
$\dot{m}$	: mass production rate [$\mathrm{kg/s}$]
N	: upper limit [-]
p	: pressure [bar]
P	: Probabiliry Density Function PDF [-]
$\dot{q}$	: heat flux [$\mathrm{W/m^2}$]
S	: source term [$\mathrm{W/m^3}$]
T	: temperature [K]
t	: time [s]
u	: velocity [$\mathrm{m/s}$]
x	: spatial coordinate [m]
Y	: species mass fraction [-]
Z	: mixture fraction [-]
Z''^2	: mixture fraction variance [-]
α	: strain rate [$\mathrm{1/s}$]
ζ	: normalized enthalpy [-]
λ	: thermal conductivity [$\mathrm{W/(m \cdot K)}$]
μ	: optimization damping factor [-]
ν	: stoichiometric coefficient [-]
ρ	: density [$\mathrm{kg/m^3}$]
ϕ	: generic variable [-]
χ	: scalar dissipation rate [$\mathrm{1/s}$]
$\dot{\omega}$	: molar production rate [$\mathrm{mol/s}$]

Subscripts

ad	: adiabatic
c	: cell
fu	: fuel
k	: species index
min/max	: minimum/maximum
ox	: oxidizer
sp	: species
st	: stoichiometric
tar	: target value
$wall$	: wall

1. INTRODUCTION

Turbulent combustion processes are present in a large number of engineering problems. Of particular interest are the applications, which include flame-wall interaction and convective heat losses. Wall-confined reacting flows subject to heat losses to the wall are always found in gas turbine combustion chambers and rocket engine thrust chambers. In both cases, the interaction of the hot gas and the wall leads to heat loads that must be taken into account in the design process of the engine.

The proper design of the cooling system is especially crucial in the case of rocket engines. The

high velocity flows with adiabatic temperature exceeding 3500 K within the thrust chamber can lead to extreme heat flux values of up to ~150 MW/m^2 in the nozzle due to the steep temperature gradients [1]. Moreover, the tendency in liquid rocket engines is to use high operating pressures in order to achieve higher specific impulse, compactness of the chamber and a higher nozzle expansion ratio for a given exhaust diameter [2]. Increasing the chamber pressure however, has a direct impact on the wall heat loads, since the heat transfer coefficient is approximately linearly proportional to the chamber pressure ($\dot{q} \sim p^{0.8}$) [3]. An insufficient cooling of the structure would rapidly lead to a mechanical damage of the flight hardware and a mission failure. Therefore, the design of thrust chambers has to meet many conflicting requirements simultaneously such as high performance, reliable cooling, low weight, structural safety and costs.

Measurements of the wall heat loads with experimental methods in the design process of a rocket engine can be done with high-cost firing tests. In order to reduce the development costs of new rocket engines, expensive trial-and-error has to be kept at a minimum. For that reason, numerical methods for the accurate description of the combustion and heat transfer processes are necessary. At the same time however, the computational cost of these methods should not be too high, in order to allow for fast estimations of the performance and the heat loads in the early design process of the components and systems.

The simulation of turbulent combustion within rocket engines usually needs the incorporation of detailed chemistry. In engineering applications using RANS, the Finite Rate Model and the Eddy Dissipation Concept are often utilized to account for the chemical reactions between the species. These detailed models however require the solution of $N_{sp} - 1$ additional equations for the N_{sp} species being modeled. For that reason, efforts have been made in order to reduce the complexity of the turbulent combustion simulations by introducing simplified models with a smaller number of equations, which directly accelerates the computation. A common method used for the simulation of H_2/O_2 rocket engines is the assumption of chemical equilibrium with turbulence/chemistry interactions which is justified by the high pressure and high temperature combustion environment as well as by the fast timescales of the hydrogen combustion reactions.

In the case of hydrocarbon combustion such as CH_4/O_2 however, the assumption of chemical equilibrium is no longer valid. The increased complexity of the chemical mechanism, combined with the larger timescales of chemical kinetics give rise to non-equilibrium effects. In order to overcome this insufficiency of the equilibrium model, the flamelet model has been widely used in many rocket engine simulations using CH_4/O_2 as propellants. The classical Flamelet model, developed by Peters [4] is able to capture the departure from the chemical equilibrium, but needs to be extended in order to account for changes in the gas composition in the presence of low-enthalpy regimes, as is the case in cooled rocket engine walls. In the present study, an extension of the Flamelet model is undertaken, in order to capture non-adiabatic effects in the presence of wall heat losses. Two methods for the introduction of the non-adiabatic table generation are presented and the results are compared. A closer investigation of the tabulated results gives important insights into the effect of lower enthalpy onto the concentration, thermodynamic and transport properties of the gas mixture.

2. FLAMELET COMBUSTION MODEL

In many practical engineering applications, including rocket thrust chambers, the equilibrium model has been applied in order to describe the occurring chemical processes. For the description of propellants with complex chemistry and slow timescales however, the Flamelet model has been widely implemented, since it is able to capture non-equilibrium effects.

According to the Flamelet turbulent combustion model, the turbulent flames are viewed as an ensemble of local flame structures with laminar nature (laminar flamelets). These flamelets are affected by the turbulent flow by being stretched and wrinkled but without changing their properties. This assumption is valid when the relevant chemical scale is short compared to the convection and diffusion time scales, since under this conditions combustion takes place within the asymptotically thin flamelets, embedded in the turbulent flow [5].

This enables the decoupling of the chemical and turbulent processes and hence a significant reduction in computational time, while still allowing for the use of a detailed chemical reaction

mechanism. Specifically, the calculation of the laminar flamelets is carried out in a pre-processing step, while the presence of turbulent fluctuations is accounted for by a Presumed Probability Density Function (PPDF) (Peters [6]). The thermochemical data of the turbulent flamelet solutions can then be tabulated as a function of a reduced set of scalars, which results in significant speed-up of the simulation.

Two main methods for the calculation of the one-dimensional local laminar flame structures (i.e. laminar flamelets) exist:

- Flamelet equations in the mixture fraction space
- Counterflow diffusion flame in physical space

2.1 Flamelet equations

The Flamelet equations consist of the governing equations for the chemical species and the temperature (or enthalpy) of the one-dimensional flame structure. To derive those equations, Peters [4], [6] applied a coordinate transformation by introducing a coordinate system that is attached to the flamelet structure. The spatial coordinate is hence replaced by the mixture fraction Z. This leads to a simplification since only the gradients perpendicular to the iso-surface of the mixture fraction are dominant and all gradients on the iso-surface can be neglected [6]. The resulting equations are given as follows under the assumption of unity Lewis number for all chemical species [5].

$$\frac{\partial Y_k}{\partial t} = \frac{\chi}{2}\frac{\partial^2 Y_k}{\partial Z^2} + \frac{\dot{m}_k}{\rho} \tag{1}$$

$$\frac{\partial T}{\partial t} = \frac{\chi}{2}\frac{\partial^2 T}{\partial Z^2} - \frac{1}{\rho c_p}\sum_{k=1}^{N_{sp}} \dot{m}_k h_k \tag{2}$$

where Y_k, $\dot{m}_k$ and h_k denote the mass fraction, mass production rate and specific enthalpy of species k respectively, while T, ρ, c_p stand for the temperature, density and constant-pressure specific heat capacity. Several formulations for the temperature equation exist (Peters [5], [6], Pitsch et al. [7], Kim et al. [8], Barths [9]), however the formula from Peters [5] is shown in the present work (Eq. 2). The scalar dissipation rate χ represents the diffusion time scale and is a measure for the departure of the local flame structure from chemical equilibrium. Values of the scalar dissipation close to $\chi = 0\ 1/s$ are equivalent to the equilibrium solution, whereas higher values for χ induce a larger departure from equilibrium. This characteristic quantity in the description of nonpremixed turbulent combustion is also able to describe the extinction limit of the flame. When it reaches the critical value χ_{ex}, the non-equilibrium effects are so dominant that quenching of the flame occurs. A typical profile for the scalar dissipation rate is given by the parametric distribution in Eq. 3 (Peters [6]), whereas other formulations are shown in Pitsch et al. [7] and Kim et al. [8].

$$\chi(Z) = \chi_{st}\exp[2(\mathrm{erfc}^{-1}(2Z_{st}))^2 - 2(\mathrm{erfc}^{-1}(2Z))^2] \tag{3}$$

χ_{st} and Z_{st} represent the scalar dissipation and mixture fraction at stoichiometry and erfc^{-1} the inverse of the complementary error function.

The boundary value problem defined by Eqs. 1, 2 can be solved in steady state conditions ($\partial Y_k/\partial t = \partial T/\partial t = 0$) for different values of χ_{st}, resulting in a tabulation of the resulting temperature and species mass fractions for the laminar flamelets: $T, Y_k = f(Z, \chi_{st})$.

2.2 Counterflow diffusion flame

Apart from solving the Flamelet equations in the mixture fraction space, it is possible to calculate a 1D laminar counterflow diffusion flame in order to obtain the temperature and mass fraction profiles along the flame front. In a counterflow diffusion flame, oxidizer and fuel enter the domain from two inlets placed opposite to each other and react along the axis. Counterflow diffusion flames are very often also used experimentally because they represent an essentially one-dimension diffusion flame structure. A schematic illustration of a counterflow diffusion flame is shown in Figure 1.

In order to calculate a counterflow diffusion flame, the conservation equations for mass, radial momentum, energy and species have to be solved. The governing equations can be found in Cantera [10]. Since the governing conservation laws are solved in the physical space, the scalar dissipation rate is not part of the equations. It can be calculated *a posteriori* as a function of the flow's strain rate α as shown in Peters [6] and Kim et al. [11]. Typical definitions of α are the maximum or the average velocity gradient in the flow field and the velocity gradient at the stoichiometric point [12]. Therefore,

instead of defining χ_{st} a priori as in the case of the Flamelet equations, the mass flows or velocities at the fuel and oxidizer inlets are modified in order to achieve the desired value of α (i.e. χ_{st}). In case the targeted and the real values of the scalar dissipation rate do not match, the boundary conditions are modified and the calculation is repeated.

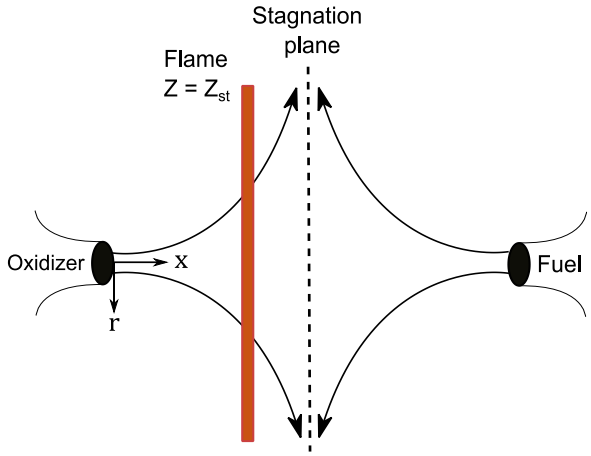

Figure 1: Schematic illustration of a counterflow diffusion flame.

Upon successful solution of the flame equations, a profile of temperature and species mass fractions (along with other quantities such as velocity) is obtained as a function of the axial position. For the tabulation however, a transformation to the Z-space is required. Although several strategies for that exist, the most general in the case of hydrocarbon combustion is the one defined in Pitsch et al. [7], since it accounts for the presence of intermediate species. In each cell of the counterflow flame domain, the mixture fraction is obtained by Eq. 4.

$$Z = \frac{\frac{Z_C}{\nu_C M_C} + \frac{Z_H}{\nu_H M_H} + \frac{2\left(Z_{O,ox} - Z_O\right)}{\nu_O M_O}}{\frac{Z_{C,fu}}{\nu_C M_C} + \frac{Z_{H,fu}}{\nu_H M_H} + \frac{2Z_{O,ox}}{\nu_O M_O}} \qquad (4)$$

where Z_i are the element mass fractions of C, H, and O respectively and ν_i the coefficients in a global reaction of the form

$$\nu_C \mathrm{C} + \nu_H \mathrm{H} + \nu_O \mathrm{O} \rightarrow \mathrm{Products} \qquad (5)$$

2.3 PDF integration

In both the solution of the Flamelet equations and the solution of the counterflow diffusion flame, a laminar table of the form $T, Y_k = f(Z, \chi_{st})$ is obtained. Of course further quantities such as density, transport properties etc. can be also tabulated since they are simply a function of the gas composition Y_k and the thermodynamic state (h, p). In order to include the effect of the Turbulence Chemistry Interaction (TCI) on the flamelets, a PPDF integration takes place using the joint PDF $P(Z, \chi_{st})$. In the present study the Favre averaged values for temperature, species mass fractions and heat capacity are calculated according to Eq. 6.

$$\tilde{\phi} = \int_0^\infty \int_0^1 \phi(Z, \chi_{st}) \cdot P(Z, \chi_{st}) \cdot \mathrm{d}Z\mathrm{d}\chi_{st} \qquad (6)$$

whereas for the transport properties (viscosity and thermal conductivity) a Reynolds averaging is used as described by Kim et al. [13].

$$\bar{\phi} = \bar{\rho} \int_0^\infty \int_0^1 \frac{\phi(Z, \chi_{st})}{\rho(Z, \chi_{st})} \cdot P(Z, \chi_{st}) \cdot \mathrm{d}Z\mathrm{d}\chi_{st} \qquad (7)$$

$$\bar{\rho} = \frac{1}{\int_0^\infty \int_0^1 \frac{1}{\rho(Z, \chi_{st})} \cdot P(Z, \chi_{st}) \cdot \mathrm{d}Z\mathrm{d}\chi_{st}} \qquad (8)$$

The assumption of statistical independence can be used to decouple the multidimensional PPDF yielding $P(Z, \chi_{st}) = P(Z) \cdot P(\chi_{st})$. For $P(Z)$, a β-PDF is usually used, the shape of which is determined by the values of $\tilde{Z}$ and its variance $\widetilde{Z''^2}$, although a Gauss distribution has also been applied in previous studies. For $P(\chi_{st})$, a Dirac delta function or a log-normal distribution are implemented [6].
The Flamelet calculations (laminar Flamelet generation and PDF integration) are usually carried out for several values of pressure, leading to a tabulation of the gas properties as in Eq. 9.

$$\tilde{\phi} = f(\tilde{Z}, \widetilde{Z''^2}, \tilde{\chi}_{st}, \tilde{p}) \qquad (9)$$

2.4 Frozen Flamelet

The Flamelet equations as well as the governing equations of the counterflow diffusion flame are adiabatic. This means that the resulting profiles for species mass fractions and temperature correspond

to a specific adiabatic enthalpy profile. Under the assumption of unity Lewis number this enthalpy profile is described as

$$h_{ad}(Z) = h_{ox} + Z(h_{fu} - h_{ox}) \qquad (10)$$

and therefore corresponds to a linear function between the boundary values of fuel and oxidizer.
In most engineering applications the flow exchanges heat with its surrounding, and hence not all points of the flow are in adiabatic conditions.
In order to account for the different enthalpy, the usual extension of the adiabatic Flamelet model is the concept of "frozen" Flamelet. According to this concept, the species concentrations are assumed to be constant for all enthalpy levels and equal to the concentration at adiabatic conditions. This assumes that the change in enthalpy does not affect the reaction paths in the chemical mechanism and does not change the composition of the gas. The only effect of the non-adiabatic enthalpy level is to change the temperature, the transport and thermodynamic properties of the gas, to render the calculation thermodynamically consistent. Physically it can be interpreted as a cooling down of burned products while ignoring any recombination effects that may take place. Therefore the Flamelet tabulation is extended by a new dimension according to Eqs. 11, 12.

$$\tilde{Y}_k\left(\tilde{Z}, \widetilde{Z''^2}, \tilde{\chi}_{st}, \tilde{p}, \tilde{h}\right) = \tilde{Y}_k\left(\tilde{Z}, \widetilde{Z''^2}, \tilde{\chi}_{st}, \tilde{p}, \tilde{h}_{ad}\right) \qquad (11)$$

$$\tilde{\phi}\left(\tilde{Z}, \widetilde{Z''^2}, \tilde{\chi}_{st}, \tilde{p}, \tilde{h} \neq \tilde{h}_{ad}\right) = f(\tilde{Y}_k, \tilde{p}, \tilde{h}) \qquad (12)$$

In the presence of cooled walls, which is the case in most rocket engine thrust chamber simulations, this method fails to predict the increase in recombination reactions which occur due to the lower enthalpy environment. The accurate description of the heat flux in the wall requires taking this effect into account and therefore an extension of the Flamelet model to non-adiabatic calculations was developed.

3. NON-ADIABATIC EXTENSION OF THE FLAMELET MODEL

Several approaches for the extension of the Flamelet model to account for non-adiabatic effects have been developed in the past. Lee et al. [14] modeled the wall heat losses by including a source term in the unsteady Flamelet equations, thereby introducing a convective heat loss process by means of a Nusselt-number correlation. Marracino et al. [15] focused on the effect of radiative losses on the Flamelet profiles by adjusting the boundaries of oxidizer and fuel, whereas Proch et al. [16] reduced the chemical heat source term in the energy equation of the counterflow diffusion flame by a constant factor. Wu et al. [17] on the other hand applied a modified thermal boundary condition to the counterflow flame in the composition space in the form of a permeable wall. A summary of those methods can also be found in Frank et al. [18]

3.1 Enthalpy profiles

To include the effects of sensible enthalpy decrease due to cooled walls and due to expansion in the nozzle, the enthalpy values should be first defined, for which the Flamelet table is generated. For this reason the normalized enthalpy variable ζ can be defined as in the work of Bilger [19]:

$$\zeta = \frac{h - h_{min}(Z)}{h_{max}(Z) - h_{min}(Z)} \qquad (13)$$

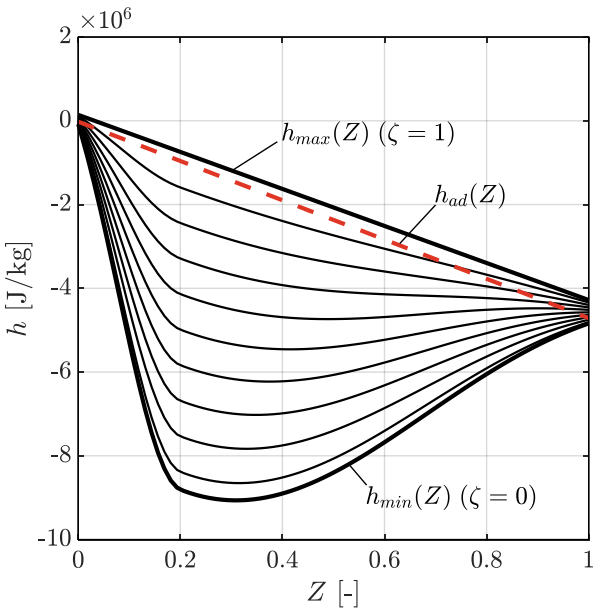

Figure 2: Enthalpy profiles in mixture fraction space.

The h_{max} and h_{min} profiles can be defined arbitrarily but ought to be chosen in order to contain all the energy loss or gain within the domain of interest. In the frame of this work, the empirical profile defined by Kim et al. [13] was used for h_{min} with slightly modified coefficients. For h_{max}, adiabatic profiles were

implemented, corresponding to temperatures at the inlets of oxidizer and fuel equal to 450 K. An example for CH_4/O_2 enthalpy profiles between the h_{max} ($\zeta = 1$) and h_{min} ($\zeta = 0$) lines as well as an adiabatic profile corresponding to $T_{fu} = 270\ K$ and $T_{ox} = 275\ K$ are shown in Figure 2.
The non-adiabatic extension of the Flamelet model aims at obtaining profiles for mass fractions, temperature and the resulting thermochemical properties of the gas corresponding to enthalpy profiles with heat loss (and heat gain) like the ones in Figure 2. In the present work, two methods for the non-adiabatic extension of the Flamelet model were implemented.

3.2 Source term method

The first method involves the introduction of a source term in the heat equation of the counterflow diffusion flame. For the solution of this 1D counteflow stagnation flow, the open-source software Cantera was utilized [10]. The modified energy equation is shown in Eq.14.

$$\rho c_p \frac{dT}{dt} = -\rho c_p u \frac{dT}{dx} + \frac{d}{dx}\left(\lambda \frac{dT}{dx}\right) - \sum_{k=1}^{N_{sp}} \dot{m}_k h_k - \sum_{k=1}^{N_{sp}} j_k c_{p,k} \frac{dT}{dx} - \boldsymbol{S(x)} \quad (14)$$

The axial coordinate is defined as x, whereas the velocity is u and j_k represents the diffusion flux of species k into the mixture according to Fick's law.
The mass production rate $\dot{m}_k$ is the product of the molar mass M_k and the molar production rate $\dot{\omega}_k$ as in Eqs. 1 and 2.
The source term $S(x)$ is defined as a function of the axial coordinate and it is modified iteratively until the desired enthalpy profile is achieved.
The first step in order to achieve that is to solve an adiabatic counterflow diffusion flame problem (i.e. with $S(x) = 0$ and obtain the enthalpy profile along the axial coordinate $h_{ad}(x)$, which can be translated to $h_{ad}(Z)$, with the transformation $Z(x)$ as described in Section 2.2. Note, that in this case the adiabatic profile, does not have the linear profile shown in Eq. 10, since the Lewis number of the species are not necessarily equal to unity, and hence differential diffusion effects come into play.
The first estimation for the source term is simply

$$S^1(x) = C \cdot \left(h_{ad}(x) - h_{tar}(x)\right) \quad (15)$$

With C representing an empirical constant and $h_{tar}(x)$ being the target enthalpy in physical coordinates, transformed from $h_{tar}(Z)$. After applying the source and solving the flame problem, the new enthalpy is obtained. The new source at iteration $i+1$ is defined as

$$S^{i+1}(x) = S^i(x) + C \cdot \left(h^i(x) - h_{tar}(x)\right) \quad (16)$$

The process is iterated until the difference $h^i(x) - h_{tar}(x)$ satisfies a pre-defined tolerance for all cells in the computational domain.

Apart from the simple proportional control of Eq. 16, the more complex Levenberg-Marquardt algorithm [20], [21], [22] was used for the update of the source term in each iteration. For its implementation, the Jacobi (or sensitivity) matrix J was calculated, defined as

$$J = \begin{bmatrix} \frac{\partial h(x_1)}{\partial S(x_1)} & \cdots & \frac{\partial h(x_1)}{\partial S(x_{N_c})} \\ \vdots & \ddots & \vdots \\ \frac{\partial h(x_{N_c})}{\partial S(x_1)} & \cdots & \frac{\partial h(x_N)}{\partial S(x_{N_c})} \end{bmatrix} \quad (17)$$

where N_c represents the number of cells in the computational domain. The Jacobi matrix was calculated with the forward finite difference method. Updating the source term takes the form

$$S^{i+1}(x) = S^i(x) + [(J^i)^T J^i + \mu^i I]^{-1} (J^i)^T \cdot \left(h^i(x) - h_{tar}(x)\right) \quad (18)$$

With the diagonal matrix I and the damping factor μ^i accounting for the fact that this inverse problem is ill-conditioned, i.e. $|(J^i)^T J^k| \approx 0$.
Both methods showed similar computational demands, with the lower number of iterations needed for the Levenberg-Marquardt method being counteracted by the computational cost of calculating the Jacobi matrix. The solution of the counterflow diffusion flame was found to be time-consuming for very low χ values and high pressures even for the adiabatic cases.

3.3 Enthalpy profile method

The source term method presented in Section 3.2 could also be implemented in the energy Flamelet equation (Eq. 2) and be solved in mixture fraction space. However, in the present work another method is presented, which was also implemented in the work of Kim et al. [13].
The idea is based on replacing the energy Flamelet equation (Eq. 2) by imposing an enthalpy profile as an equality constraint in the mixture space frame. By omitting the energy equation, the Flamelet calculation is reduced to a boundary value problem consisting of the mass fraction equation (Eq. 1) and an optimality constraint:

$$\frac{\partial Y_k}{\partial t} = \frac{\chi}{2}\frac{\partial^2 Y_k}{\partial Z^2} + \frac{\dot{m}_k}{\rho} \tag{19}$$

$$h(Z) = h_{tar}(Z) \tag{20}$$

Defining the linear profile of Eq. 10 as the desired enthalpy profile, the set of Eqs. 19, 20 becomes equivalent to the system of Eqs. 1 and 2. Applying any other profile below (or above) the adiabatic enthalpy, corresponds to a heat loss (or gain) and the equations can be solved without loss of generality.
For the solution of the resulting boundary value problem, a new methodology was implemented based on an operator splitting technique by Strang [23] and Yanenko [24]. The boundary value problem in Eq. 19 consists of a transport term (diffusion term with diffusion constant $\chi/2$) and a highly nonlinear kinetics term.
By employing the operator splitting, the nonlinear algebraic equations resulting from the discretization of Eq. 19 are broken into two smaller systems:

- A kinetics equation at each cell in the Z-space, decoupled from other cells (initial value problem)
- A diffusion equation for each chemical species, decoupled from the mass fractions of the other species (parabolic problem)

The solution of the two problems is alternated repeatedly making it possible to match the accuracy of the fully coupled problem. The algorithm was implemented in Matlab, using Cantera for the chemical calculations.

1st step: Kinetics (ideal reactors system)
For each individual cell in the 1D domain, the kinetics part of the equation is solved:

$$\frac{\partial Y_k}{\partial t} = \frac{\dot{m}_k}{\rho} \tag{21}$$

This corresponds to a constant enthalpy/constant pressure ideal reactor. The enthalpy of the reactor is defined by the equality constraint (Eq. 20) and the pressure level of the current Flamelet calculation is used. In order to ensure that the enthalpy remains constant over the time integration of Eq. 21, a temperature equation is also solved as in Eq. 22

$$\frac{\partial T}{\partial t} = -\frac{1}{\rho c_p}\sum_{k=1}^{N_{sp}} \dot{m}_k h_k \tag{22}$$

The equation system of the ideal batch reactor (Eqs. 21, 22) is solved for a time duration of $dt/2$, with dt being the global time step of the simulation [23]. The integration of the ODE system was performed using the implicit variable order solver "*ode15s"* [25].

2nd step: Diffusion (transport system)
For each species in the reaction mechanism, a parabolic PDE is defined, independent from the mass fractions of the other species.

$$\frac{\partial Y_k}{\partial t} = \frac{\chi}{2}\frac{\partial^2 Y_k}{\partial Z^2} \tag{23}$$

The diffusion equation was discretized using a central difference scheme and the time integration was performed with an implicit backwards Euler scheme. The integration of this step is performed for a time interval dt. During the integration, the temperature remains constant and has to be updated at the end, to account for the changes in the species concentration due to diffusion. For each cell in the mixture fraction space, using the thermodynamic data of the chemical mechanism:

$$T(Z) = f\big(Y_k(Z), h(Z)\big) \tag{24}$$

3rd step: Kinetics (ideal reactors system)
Finally, the ideal reactor is solved again for a time duration of $dt/2$ as in Step 1.
The process is iterated until the solution converges to a steady state, i.e. until the transient term (residual) drops under a pre-defined tolerance. The algorithm is illustrated as a flow chart in Figure 3.

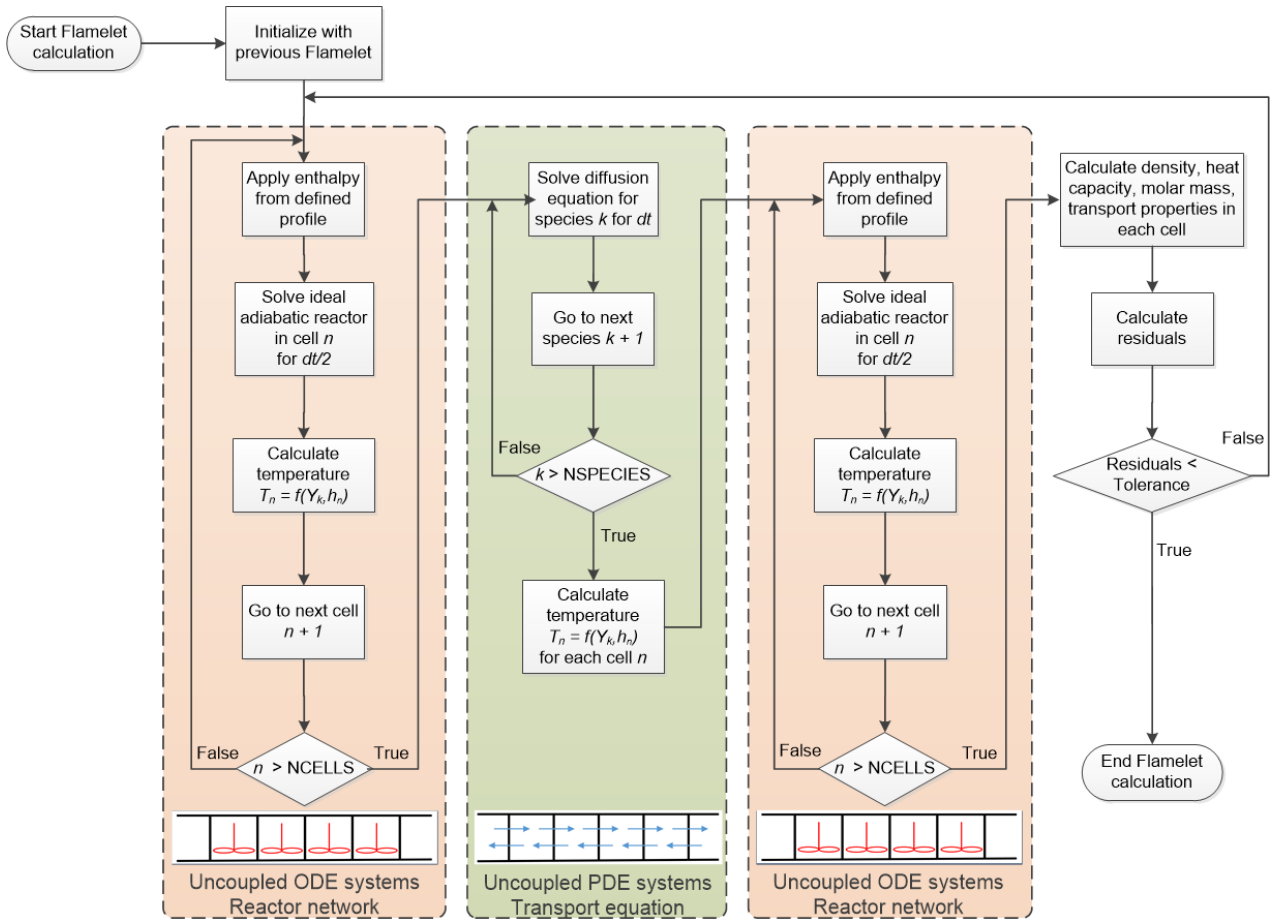

Figure 3: Flow chart of the splitting algorithm for the solution of Flamelet equations.

A validation of the method was carried out by comparing the resulting temperature and mass fraction profiles with the ones produced by the commercial ANSYS Fluent Flamelet generator [26]. The validation was carried out only for adiabatic conditions, since Fluent is only able to perform frozen calculations. However, since the adiabatic enthalpy profile is not a special case of the enthalpy prescription method, but simply one of the infinite realizations the operators splitting algorithm is expected to be reliable for all other enthalpy levels.

4. FLAMELET RESULTS

4.1 Comparison of counterflow diffusion flame and Flamelet equations

The main differences between the two approaches for the calculation of adiabatic Flamelet libraries have been summarized in Pitsch et al. [7]. In the simplified Flamelet equations, the effects of differential diffusion are ignored due to the $Le_i = 1$ assumption. On the other hand, for the solution of the counterflow diffusion flame, any model for the calculation of the diffusion coefficients can be adapted. In the present case, a mixture averaged diffusion coefficient is used for the mixture and the individual species coefficients are calculated with the kinetic theory according to Bird [27] as implemented in Cantera [10].

The main effect of the different diffusion properties between the Flamelet equations and the Cantera counterflow flame is an inconsistency in the resulting enthalpy profile for the two cases. The absence of the unity Lewis number assumption in the general case of a counterflow diffusion flame results in a non-linear enthalpy profile in the mixture fraction space. This effect is illustrated in Figure 4, where three counterflow diffusion flames were carried out at a pressure level of 20 bar and a scalar dissipation rate of 100 $1/s$ for pure methane (275 K) and pure oxygen (270 K) at the inlets. For all cases, the mechanism by Slavinskaya et al. [28] was implemented.

An adiabatic case using the standard mixture averaged diffusion coefficients was compared to an also adiabatic case with diffusion coefficients according to $Le = 1$. The solver Cantera does not include this option by default and hence the option was implemented in the source code. Additionally, a non-adiabatic simulation using the source term as defined in Section 3.2 was applied using the mixture averaged diffusion model. A linear profile was applied as a target enthalpy curve. Apart from the counterflow diffusion flame results, a laminar flame using the Flamelet equations with the method of enthalpy prescription (Section 3.3) is also shown.

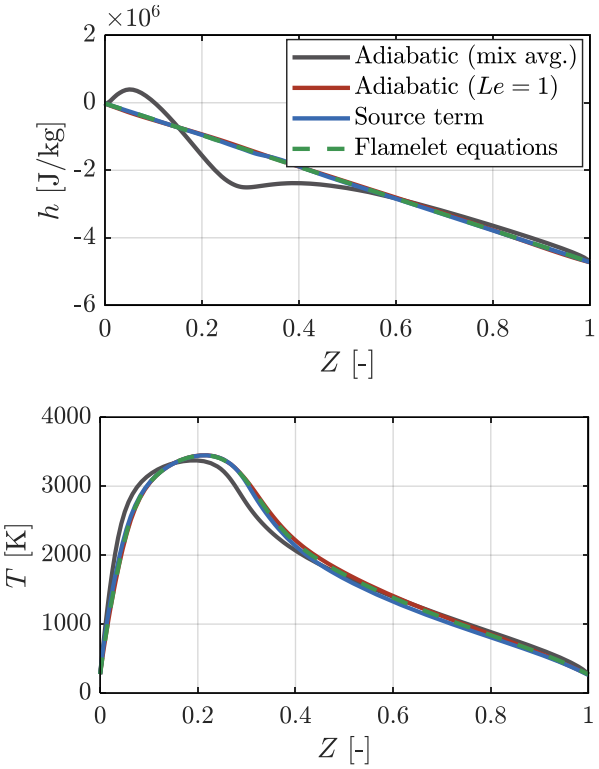

Figure 4: Enthalpy (up) and temperature (down) profiles for different realizations of the adiabatic Flamelet calculation.

As expected, solving the counterflow diffusion flame with the diffusion coefficients from kinetic theory and mixture averaging, yields a non-linear enthalpy profile. Specifically, the enthalpy appears to be higher than the linear case close to the oxidizer and lower downstream of the stoichiometric point. For the remaining three cases, the profile remains linear. The corresponding temperature also shows some differences with the most notable one being that the maximal temperature is below the one predicted by a linear enthalpy profile.

In the case of the species concentrations, one can observe that the three implementations in Cantera (mixture averaged diffusion, $Le = 1$ and source term optimization) show different results. The discrepancy between the standard approach (adiabatic with mixture kinetic theory averaged properties) and the rest can be easily attributed to the difference in enthalpy profiles and corresponding temperature. The $Le = 1$ and source term approaches however have the same enthalpy profile and very similar temperature profiles. Apparently, despite the negligible differences in temperature, the discrepancies in species concentrations due to different transport values are measurable. Finally, the result coming from the Flamelet equations appears to be identical to the $Le = 1$ Cantera flame. This is easily understood, since the simplified Flamelet equations (Eqs. 1, 2) represent the transformation of the counterflow flame equations to the mixture fraction-based coordinate system under the assumption of unity Lewis number.

The differences between the different approaches are well understood. The $Le = 1$ implementation of the counterflow diffusion flame corresponds to the solution of the Flamelet equations. For the calculation of non-adiabatic enthalpy profiles, the source term is needed in the physical space. The benefit of solving the equations in physical space is that one can include detailed diffusion properties of the mixture without being restricted by the unity Lewis number assumption. Implementing the same diffusion model in the mixture fraction space would involve a much more complex set of Flamelet equations (Pitsch et al. [7]). However, the tabulated differences in all those approaches remain well within 10% in the tabulated values of species concentrations and temperature. For that reson, in the present work the Flamelet equation approach will be used for the further investigations. The main reason is the faster computational times produced by the application of the splitting algorithm as explained in Section 3.3. The calculations were repeated for several pressure levels which are relevant for rocket engine applications, from 1 bar up to 80 bar. All pressures showed similar results and therefore only the chosen level of 20 bar (representative for small scale experimental rocket engines) is presented in this work.

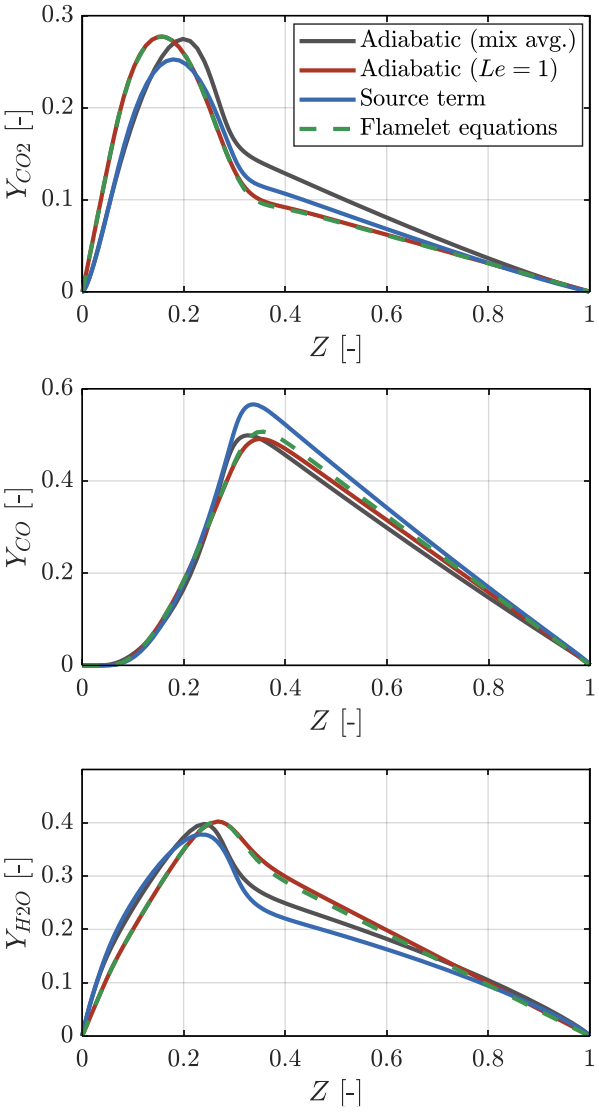

Figure 5: Species concentrations for different realizations of the adiabatic Flamelet calculation.

4.2 Comparison of frozen and non-adiabatic Flamelet

Including non-adiabatic effects in the Flamelet table generation enables capturing the effect of reactions occurring at low enthalpy levels. Such reactions are taking place along the cooled walls of rocket combustion chambers and tend to increase the observed heat flux. Specifically, the reduced enthalpy environment suppresses dissociation processes since not enough energy is present to break the chemical bonds. This translates to an increase of recombination processes and a consequent increase in the energy release. This energy release is a result of the lower building enthalpy of the stable products of the recombination reactions. A dominant reaction in the case of hydrocarbon combustion and specifically CH_4/O_2 engines is the recombination of CO and O to CO_2.

In order to understand the effect of the non-adiabatic Flamelet formulation, the results of a frozen chemistry table are compared to the ones from the solution of the enthalpy-dependent Flamelets. The load point chosen corresponds to 20 bar CH_4/O_2 combustion and a scalar dissipation rate of 0.1 $1/s$. A low value for χ was chosen, since the effects of enthalpy loss are mainly dominant in the vicinity of the wall, where the scalar dissipation has small values approaching to zero. The maximum and minimum enthalpy profiles are the ones from Figure 2, with 17 levels placed in between.

The temperature results shown in Figure 6 illustrate the main differences between the two approaches. In the frozen case, an enthalpy reduction has a higher temperature decrement as a consequence. This occurs due to the lower specific heat capacity of the radicals compared to the stable molecules such as CO_2. In the case of the non-adiabatic model however the heat released from the recombination reactions leads to a smaller temperature decrease in the lower enthalpy levels.

When frozen chemistry is assumed, the lowest enthalpy levels can lead to unphysical temperatures even below 0 K. This is due to the absence of recombination heat release. The species present in the frozen composition cannot exist in such a low enthalpy environment and to avoid that, a temperature cutoff at 200 K was set in the calculation. This explains the flat line at the lowest energy level in the frozen case.

The differences between the two approaches are mainly present close to stoichiometry, whereas for fuel-richer regions the discrepancies are reduced. Since in most practical CH_4/O_2 rocket engine applications the mixture is fuel rich and since in typical co-axial injector configurations the fuel is injected on an outer annulus, the gas composition at the wall is dominantly fuel-rich. The small differences in this region explain why the conventional frozen Flamelet model is able to predict reasonable values for the wall heat fluxes when applied in CFD.

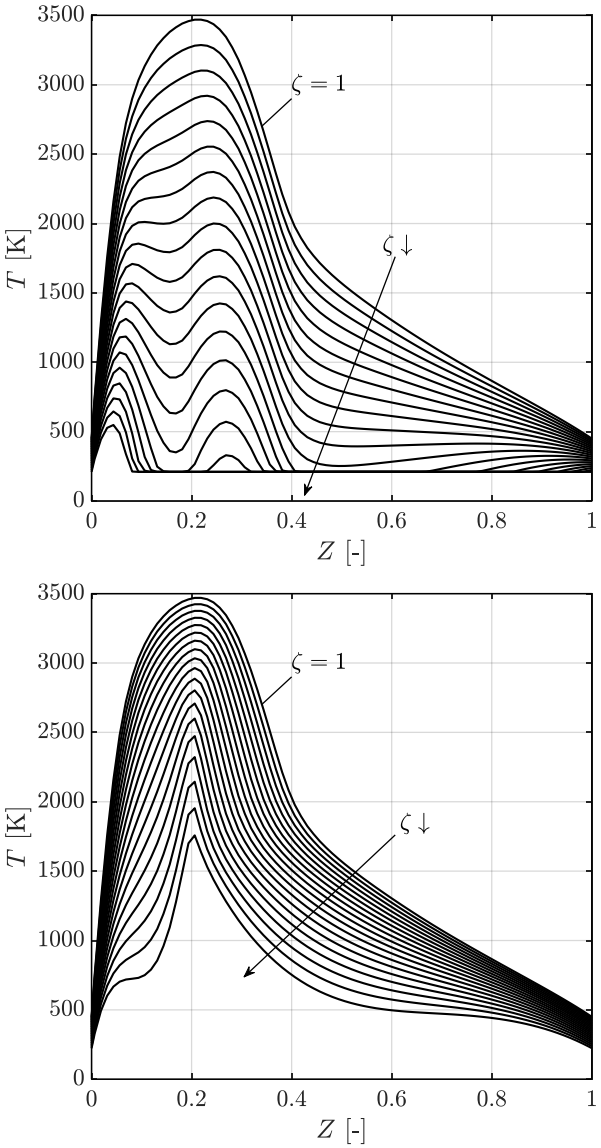

Figure 6: Temperature profiles for different enthalpy levels in the case of the frozen (up) and non-adiabatic (down) Flamelet models.

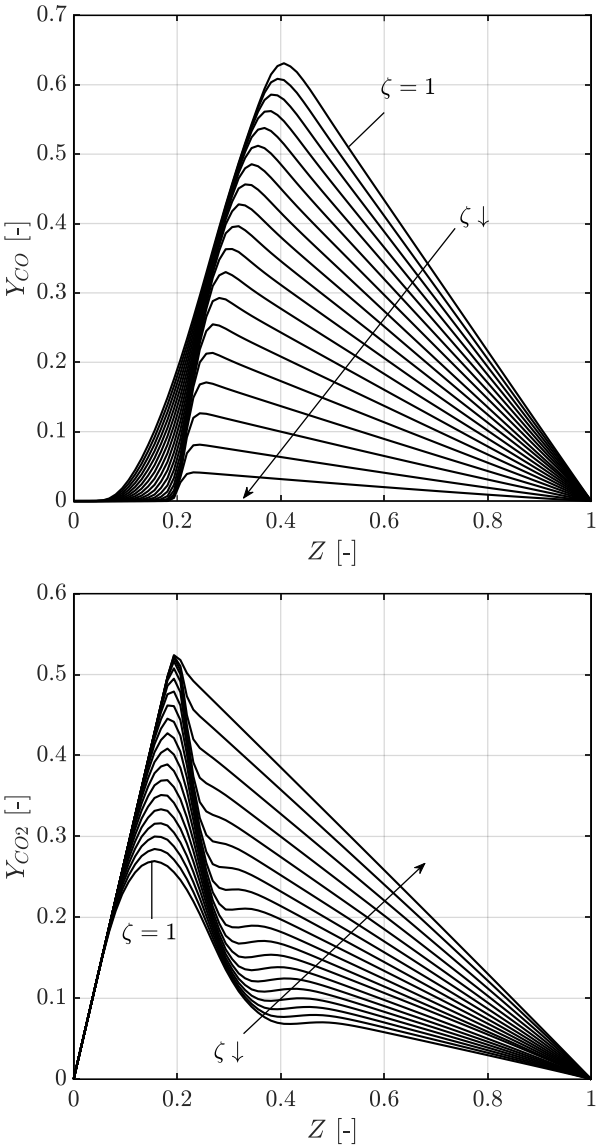

Figure 7: CO (up) and CO_2 (down) profiles for different enthalpy levels.

The results of the species concentrations for different enthalpy levels are shown in Figure 7. As expected the effect of a lower energy environment is to decrease the composition of CO and increase the CO_2 concentration. The energy release taking place in the recombination is responsible for the temperature difference in Figure 6. Note that the frozen solution corresponds to the $\zeta = 1$ lines of Figure 7, for all enthalpy levels.

The importance of the non-adiabatic Flamelet model becomes more evident when the results are compared to the equilibrium solution. Figure 8 and Figure 9 show the differences in temperature and species profiles for the three models. The equilibrium model overpredicts the production of CO_2 due to recombination effects, whereas the frozen model underpredicts it. The recombination of CO to CO_2 is a slow process, and therefore the assumption of chemical equilibrium is not applicable in hydrocarbon combustion.

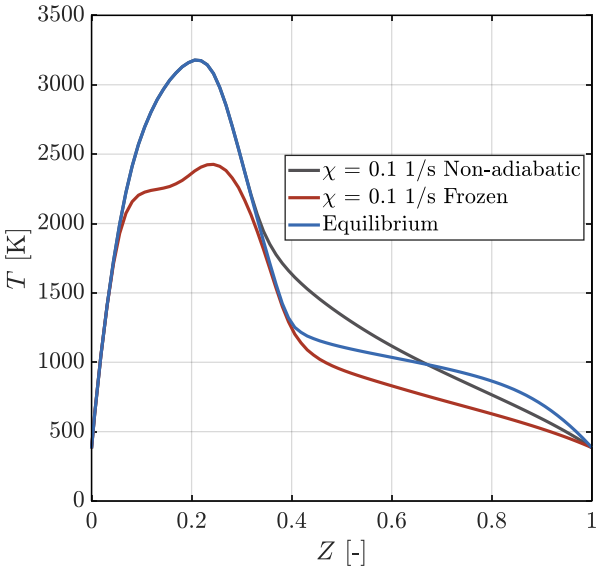

Figure 8: Temperature profile for non-adiabatic Flamelet, frozen Flamelet and chemical equilibrium for $\zeta = 0.7$.

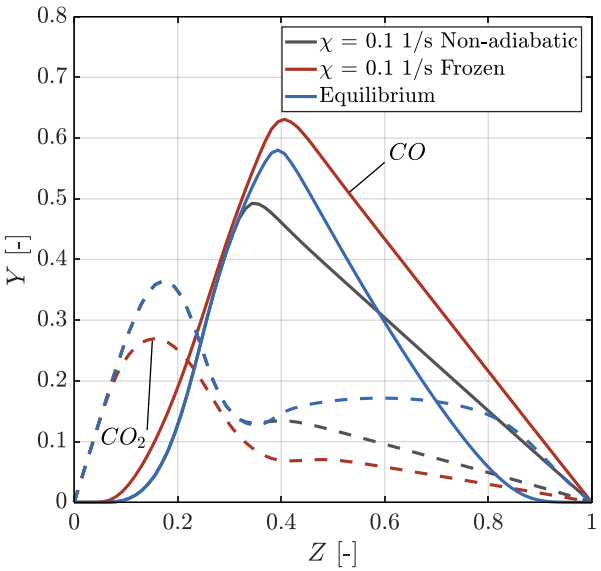

Figure 9: Species concentration profile for non-adiabatic Flamelet, frozen Flamelet and chemical equilibrium for $\zeta = 0.7$.

In order to qualitatively describe the expected differences in heat load for the two methods in a CFD calculation, the thermal conductivity and a normalized heat flux were calculated based on the tabulated Flamelet results. For the calculation of the conductivity, kinetic theory was used for the individual species and the Wilke mixing rule was implemented according to Cantera [10]. The pseudo-heat flux calculation was performed by assuming a wall temperature equal to 500 K. The resulting heat flux metric was defined by Eq. 25 and normalized by the maximal value.

$$\dot{q} = \lambda(T - T_{wall}) \qquad (25)$$

The results of the thermal conductivity shown in Figure 10 demonstrate that in fuel-rich regions the difference between the two models remains constrained.

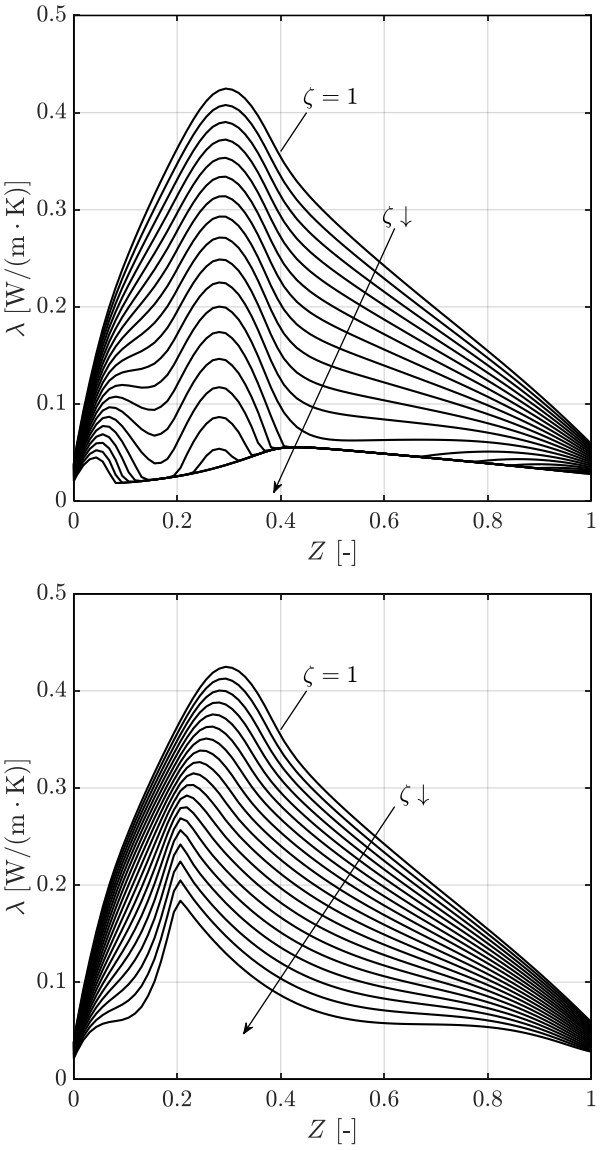

Figure 10: Thermal conductivity of the frozen (up) and non-adiabatic (down) Flamelet models.

The molecular thermal conductivity is a rather important factor in the CFD of rocket engines since it directly influences the predicted heat loads on the wall. In RANS simulations, although its significance

in the core flow is not so high due to the dominance of the turbulent fluxes (turbulent conductivity), the molecular transport strongly influences the wall boundary layer. Since the flow in the viscous sublayer is purely laminar, the wall heat flux is strongly dependent on the value of the thermal conductivity.

In order to estimate the effect on the predicted wall heat load for the two models, the normalized heat flux from Eq. 25 is shown in Figure 11. Note that every second enthalpy line is plotted for the sake of clarity and only the fuel rich region is illustrated. As expected by theory, the resulting heat flux in the case of a non-adiabatic Flamelet formulation exceeds the one from the frozen case. The differences appear to increase at lower enthalpy levels and hence should be more dominant in the simulations of strongly cooled chamber walls. Nevertheless, the differences that the two models will have in CFD cannot be exactly predicted since they are expected to have different enthalpy and mixture fraction fields which add to a further discrepancy apart from the tabulated values. A study of the model's effect on the wall heat flux and the flow inside a rocket combustion chamber is given by Perakis et al. [29].

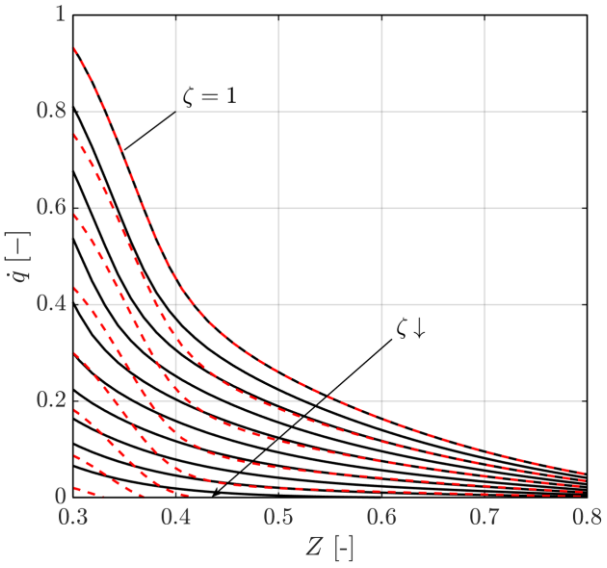

Figure 11: Normalized heat flux values for the frozen (dashed line) and non-adiabatic Flamelet model (solid line) at different enthalpy levels.

5. CONCLUSION AND OUTLOOK

The Flamelet model is a very promising method for the simulation of turbulent combustion in applications where non-equilibrium effects become significant. Its application in CFD simulations of rocket combustion engines with hydrocarbons as propellants reduces the computational time compared to more thorough approaches such as finite rate chemistry. The extension of the Flamelet model to include non-adiabatic effects is however needed to accurately predict the wall heat loads.

For the generation of non-adiabatic Flamelet tables, an extension of two existing approaches was undertaken in this work. The solution of the counterflow diffusion flame in physical coordinates was broadened by the introduction of an energy source term. By means of an optimization algorithm, arbitrary enthalpy levels were able to be achieved by modifying the source term. The benefits of this method were the capability to include any transport mechanism for the diffusion properties of the gas, without the unity Lewis number restriction. However, a poor convergence was observed for lower values of the scalar dissipation rate and higher pressures, rendering the method impractical for most applications needing a good resolution of χ in the vicinity of the wall.

The solution of the Flamelet equations in the mixture fraction space was also carried out. For the introduction of the enthalpy loss or gain, the temperature equation was substituted by a prescription of an enthalpy profile as an equality constraint. A new method of solving the resulting boundary value problem was presented, based on the splitting of the diffusion and reaction operators.

Both methods delivered similar results for the temperature and species concentrations. The differences between the established frozen Flamelet approach and the non-adiabatic one were compared. As expected, it was found that the frozen model cannot predict the recombination effects occurring at lower enthalpy levels, which lead to a significant heat release. This was confirmed by the lower temperature profiles predicted in the frozen case. In contrast, the equilibrium model, which is often used in the simulation of hydrogen engines was found to overpredict the recombination effects, effectively increasing the concentration of CO_2 in the fuel rich regions.

Finally, an estimation of the expected heat fluxes on the cooled walls of a rocket chamber was carried

out. The heat loads predicted by the frozen approach are below the non-adiabatic ones. Hence, for the correct estimation of the high heat flux in rocket thrust chambers, the non-adiabatic extension should be included in Flamelet calculations. CFD tests for the verification of the model have been planned and will give insight into the behavior of the non-adiabatic tables in high and low pressure rocket engine applications with cooled walls.

ACKNOWLEDGEMENTS

Financial support has been provided by the German Research Foundation (Deutsche Forschungsgemeinschaft – DFG) in the framework of the Sonderforschungsbereich Transregio 40.

REFERENCES

[1] G. Sutton and O. Biblarz, Rocket propulsion elements, John Wiley & Sons, 2017.

[2] G. Sutton, History of liquid propellant rocket engines, AIAA, 2006.

[3] G. Schmidt, Technik der Flüssigkeits-Raketentriebwerke, Munich: DaimlerChrysler Aerospace, 1999.

[4] N. Peters, "Laminar diffusion flamelet models in non-premixed turbulent combustion.," *Progress in energy and combustion science,* vol. 10, no. 3, pp. 319-339, 1984.

[5] N. Peters, "Laminar flamelet concepts in turbulent combustion," *Twenty-first Symposium (International) on Combustion,* pp. 1231-1250, 1986.

[6] N. Peters, Turbulent Combustion, Cambridge University Press, 2000.

[7] H. Pitsch and N. Norbert, "A consistent flamelet formulation for non-premixed combustion considering differential diffusion effects.," *Combustion and Flame,* vol. 114, no. 1, pp. 26-40, 1998.

[8] S.-K. Kim, S.-M. Kang and Y.-M. Kim, "Flamelet modeling for combustion processes and NOx formation in the turbulent nonpremixed CO/H2/N2 jet flames.," *Combustion science and technology,* vol. 168, no. 1, pp. 47-83, 2001.

[9] H. Barths, H. Pitsch and N. Peters, "Three-Dimensional Modeling of NOx and Soot Formation in DI Diesel Combustion and Pollutant Formation," in *SAE Technical Paper*, 1996.

[10] D. G. Goodwin, H. K. Moffat and R. L. Speth, "Cantera: An object- oriented software toolkit for chemical kinetics, thermodynamics, and transport processes.," 2017. [Online]. Available: http://www.cantera.org.

[11] J. S. Kim and F. S. Williams, "Structures of flow and mixture-fraction fields for counterflow diffusion flames with small stoichiometric mixture fractions.," *SIAM Journal on Applied Mathematics,* vol. 53, no. 6, pp. 1551-1566, 1993.

[12] C. K. Law, Combustion physics, Cambridge University Press, 2010.

[13] S. K. Kim, M. Joh, H. S. Choi and T. S. Park, "Multidisciplinary simulation of a regeneratively cooled thrust chamber of liquid rocket engine: Turbulent combustion and nozzle flow.," *International Journal of Heat and Mass Transfer,* vol. 70, pp. 1066-1077, 2014.

[14] D. J. Lee, S. Thakur, J. Wright and M. Ihme, "Characterization of flow field structure and species composition in a shear coaxial rocket GH2/GO2 injector: modeling of wall heat losses.," *AIAA Paper,* vol. 6125, 2011.

[15] B. Marracino and D. Lentini, "Radiation modelling in non-luminous non premixd turbulent flames," *Combustion Science and Technology,* vol. 128, pp. 23-48, 1997.

[16] F. Proch and A. M. Kempf, "Modeling heat loss effects in the large eddy simulation of a model gas turbine combustor with premixed flamelet generated manifolds.," *Proceedings of the Combustion Institute,* vol. 35, no. 3, pp. 3337-3345, 2015.

[17] H. Wu and M. Ihme, "Modeling of Wall Heat Transfer and Flame/Wall Interaction: A Flamelet Model with Heat-Loss Effects," in *9th U.S. National Combustion Meeting*, Cincinnati, Ohio, 2015.

[18] G. Frank, J. Zips and M. Pfitzner, "Construction of Libraries for Non-Premixed Tabulated Chemistry Combustion Models including Non-Adiabatic Behaviour due to Wall Heat Losses," in *Sonderforschungsbereich/Transregio 40 - Annual Report*, 2016.

[19] R. W. Bilger, "Turbulent flows with nonpremixed reactants.," in *Turbulent reacting flows*, 1980, pp. 65-113.

[20] D. W. Marquardt, "An algorithm for least-squares estimation of nonlinear parameters," *Journal of the society for Industrial and Applied Mathematics,* vol. 11, no. 2, pp. 431-441, 1963.

[21] K. Levenberg, "A method for the solution of certain non-linear problems in least squares.," *Quarterly of applied mathematics,* vol. 2, no. 2, pp. 164-168, 1944.

[22] M. N. Ozisik, Inverse heat transfer: fundamentals and applications., CRC Press, 2000.

[23] G. Strang, "On the Construction and Comparison of Difference Schemes.," *SIAM Journal on Numerical Analysis,* vol. 5, no. 3, pp. 506-517, 1968.

[24] N. N. Yanenko, The method of fractional steps., New York: Springer, 1971.

[25] L. Shampine and M. Reichelt, "The Matlab ODE Suite," MathWorks, Inc., Natick, MA, 1997.

[26] Fluent ANSYS, "Ansys Fluent theory guide," ANSYS Inc. USA, 2011.

[27] B. R. Bird, Transport phenomena, 2002.

[28] N. Slavinskaya, M. Abbasi, J. H. Starcke, A. Mirzayeva and O. J. Haidn, "Skeletal Mechanism of the Methane Oxidation for Space Propulsion Applications.," in *52nd AIAA/SAE/ASEE Joint Propulsion Conference*, 2016.

[29] N. Perakis, C. Roth und O. J. Haidn, „Simulation of a single-element rocket combustor using a non-adiabatic Flamelet model.," in *Space Propulsion*, Sevilla, Spain, 2018.